# Theoretical study of matter density distribution and elastic electron scattering form factors for the neutron-rich $^{22}$C exotic nucleus

**Adel K. Hamoudi, Raad A. Radhi, Arkan R. Ridha**

Department of Physics, College of Science, University of Baghdad, Baghdad, Iraq

Email: rifaaharkan@yahoo.co.uk

**Abstract**

The ground state proton, neutron, and matter density distributions and corresponding root-mean-square radii (rms) of the unstable neutron-rich $^{22}$C exotic nucleus are investigated by two-frequency shell model (TFSM) approach. The single-particle wave functions of harmonic-oscillator (HO) potential are used with two oscillator parameters $b_{core}$ and $b_{halo}$. According to this model, the core nucleons of $^{20}$C are assumed to move in the model space of *spsdpf*. Shell model calculations are performed with $(0+2)\hbar\omega$ truncations using Warburton-Brown psd-shell (WBP) interaction. The outer (halo) two neutrons in $^{22}$C are assumed to move in HASP (H. Hasper) model space ($2s_{1/2}$, $1d_{3/2}$, $2p_{3/2}$, and $1f_{7/2}$ orbits) using the HASP interaction. The halo structure of $^{22}$C is confirmed with $2s_{1/2}$-dominant configuration. Elastic electron scattering form factors of $^{22}$C nucleus are also investigated using the plane wave Born approximation. The effect of the long tail behavior (found in the calculated matter density distribution) on the elastic form factor of $^{22}$C is studied. The calculated matter densities and form factors of stable $^{14}$C and unstable $^{22}$C are compared. It is found that the difference between the nucleon form factors of $^{22}$C and $^{14}$C nuclei is attributed to the difference presented in the matter densities of these nuclei. Hence the difference in the matter densities of $^{22}$C and $^{14}$C nuclei mainly comes from the neutron skin of the core $^{20}$C and from the difference in the neutron density distribution of the last two neutrons in both $^{14}$C and $^{22}$C nuclei. It is concluded that elastic electron scattering from exotic nuclei can provide predictions for the near future experiments on the electron-radioactive beam colliders, where the effect of the neutron halo or skin on the charge distributions is planned to be studied.

**Key words**

*Halo Nuclei, neutron-rich nuclei, Two-frequency shell model, nuclear density distribution, elastic Coulomb form factor.*

Article info

*Received: Jan. 2012*

*Accepted: Nov. 2012*

*Published Dec.2012*

# دراسة نظرية لتوزيع الكثافة الكتلية وعوامل التشكل المرنة لأستطارة الألكترون لنواة $^{22}$C الغريبة الغنية بالنيوترونات

**عادل خلف حمودي، رعد عبد الكريم راضي، أركان رفعت رضا**

قسم الفيزياء، كلية العلوم، جامعة بغداد، بغداد، العراق

**الخلاصة**

تم دراسة توزيعات الكثافة البروتونية والنيوترونية داخل النواة بالاضافة الى الكتلية وما يقابلها من انصاف الاقطار لنواة الكاربون-22 باستخدام أنموذج القشرة ذو الترددين. استخدمت الدوال الموجية للجسيمة المفردة لجهد المتذبذب التوافقي مع قيمتين مختلفتين للثابت التوافقي واحدة للقلب ($b_{core}$) والاخر للهالة ($b_{halo}$). بناءا على هذا الانموذج، تم افتراض ان نيوكليونات القلب (الكاربون-20) تتحرك في فضاء *spsdpf* مع قطع للفضاء بمقدار $(0+2)\hbar\omega$ باستخدام تفاعل WBP.

نيوترونا الهالة افترض بانها تسبح مرة في فضاء ال HASP ($2s_{1/2}$, $1d_{3/2}$, $2p_{3/2}$, and $1f_{7/2}$) بأستخدام التفاعل HASP ومرة في المدار الصرف 1d و $2s_{1/2}$ . كما وتم تحقيق عوامل التشكل المرنة لنواة الكاربون-22 بواسطة تقريب بورن للموجة المستوية. تاثير المركبة الطويلة المستنتج في توزيع الكثافة الكتلي على عامل التشكل المرن للكاربون-22 ايضا تم دراسته ومقارنته مع النظير المستقر الكاربون-14. وجد بان الاختلاف بين عوامل التشكل النيوكليونية للكاربون-14 والكاربون-22 يعزى الى الاختلاف الموجود في توزيعات الكثافة لهذه النوى؛ حيث ان الاختلاف في هذه التوزيعات يأتي بصورة رئيسية من الطبقة النيوترونية للقلب (الكاربون-20) بالاضافة الى نيوترونا الهالة الاخيرفي الكاربون-22 . اخيرا، نتائج عوامل التشكل الكولومية المرنة للاستطارة الالكترونية المحسوبة هنا يمكن ان تزودنا بتنبؤات للتجارب المستقبلية القريبة المزمع انشاؤها في صادم الالكترون-نواة حيث يخطط فيها دراسة تاثير طبقة النيوترون او الهالة على توزيع كثافة الشحنة.

## Introduction

With the advent of novel radioactive ion beam facilities, a new interesting field in nuclear physics has been turned out. It was shown that nuclear radii can be determined from interaction cross sections of high-energy heavy-ion collisions [1]. Such approach provides a unique method for determining matter radii of unstable nuclei. The pioneering discovery in this field was noticing extraordinary enhancement in the total reaction cross section induced by unstable nuclei impinging on stable targets by Tanihata et al [1]. An abnormally matter rms radius for the neutron-rich $^{11}$Li nucleus was observed much larger than other neighboring isotopes; suggesting the existence of a long tail in nuclear matter density distribution. Afterwards, this led to the definition of neutron halo [2, 3, 4].

A neutron halo is basically a threshold effect resulting from the presence of a bound state close to the continuum; this is mainly attributed to the closeness of the Fermi level to the particle continuum. The valence nucleons could be easily scattered to the continuum states, hence and forth due to the pairing correlation. The tail of the wave function extends more outward the central nuclear confining potential well which eventually leads to the formation of a diffuse nuclear cloud surrounding the core. For the occurrence of nuclear halo, the well-accepted conditions are small binding energy and low angular momentum. The structure of halo nuclei are imagined to be composed of a tightly bound core plus one loosely nucleon or two (two-nucleon halo is called Borromean [5], since none of the binary subsystems of the core plus two nucleon are found in bound state). These nuclei are sometimes called exotic due to their large neutron ($N$) or proton ($Z$) numbers leading to unusual properties in their structures, e.g. halo and skin. In stable nuclei, the ratio $N/Z$ are restricted in between 1 to 1.5, as well as the separation energy of a nucleon, either a proton or a neutron, is almost always 6 to 8 MeV, on the other hand, the $N/Z$ can be varied from 0.6 to 4, also the separation energy can be varied from 40 MeV to 0 MeV. The half-life times for halo nuclei are in general less than one second.

Because of the rapid decay of these nuclei, it is rather difficult to make targets with them, therefore, experiments have been done in inverse kinematics (i.e., the roles of target and projectile are exchanged) with a beam of exotic nuclei incident on a stable target at radioactive ion beam (RIB) facilities.

The problem of determining the density distribution and size of halo nuclei is currently debated. The extraction of the nucleon density distribution and nuclear radius from experimental total reaction cross section of nucleus-nucleus collisions has been carried out almost exclusively by using the Glauber model in the optical-limit approximation. This is an advantage of the Glauber model that relates the cross sections of nucleus-nucleus collisions to the nuclear

density and nucleon-nucleon cross sections. Experimental values obtained from such treatment are subject to controversy [6], being sensitive to the model used to describe the reaction mechanism. The electron scattering from nuclei is a powerful tool to investigate the electromagnetic structure in stable nuclei. This is because of the relatively weak interaction of electron with nucleus which is done through the well-known electromagnetic force. Electron scattering from exotic nuclei is not presently available; the technical proposal for the construction of electron-ion collider at GSI/Germany [7] and RIKEN/Japan facility [8] will be a great opportunity to study the electromagnetic structure of these exotic nuclei in the near future.

For the two-neutron Borromean $^{22}$C halo nucleus, many theoretical and experimental studies had discussed and confirmed the halo structure and found in refs. [9, 18].

The no-core shell model (NCSM) calculations in light nuclei were applied to halo nuclei with poor agreement [19-22] for rms radii and separation energies even for large model space. This is probably related to the Gaussian fall-off of the NCSM wave functions, which does not reproduce the correct exponential tail. The limitation of no-core shell model calculations is arising from the increasing dimensionality with mass for a given model space, therefore, It will be cumbersome and very time consuming.

The two-frequency shell-model (TFSM) approach was employed successfully on halo nuclei [23, 24], for both valence energy and rms radii. Within this model, one uses harmonic-oscillator (HO) wave functions with two oscillator size parameters, $b_{core}$ and $b_{halo}$ for the core and halo orbits, respectively. This technique will enable one to work freely on each part by changing $b_{core(halo)}$ till one can get a fit with some experimental results. Unfortunately there is no application of the TFSM approach on the matter densities and elastic electron form factors for exotic nuclei. For this reason, we undertake the study of such substantial quantities for halo $^{22}$C nucleus in such approach. The elastic electron scattering form factors in this work are calculated in plane-wave Born approximation (PWBA) through matter densities obtained from the TFSM calculations. The effect of the long tail component observed in the calculated matter densities on elastic electron form factors for $^{22}$C nucleus is presented and discussed. Besides, the matter rms radii are also calculated according to this model.

**Theory**

The one-body operator of rank $\Delta J$ of the longitudinal transition density for point protons (with isospin $t_z = 1/2$) or neutrons ($t_z = -1/2$) is given by [25]:

$$\hat{\rho}^{L}_{\Delta J,t_z} = \sum_{k=1}^{A} e(t_z)\frac{\delta(r-r_k)}{r_k^2} Y_{\Delta J,M_{\Delta J}}(\Omega_{r_k}), \quad (1)$$

with

$$e(t_z) = \frac{1+2t_z(k)}{2}.$$

In Eq. (1), the superscript ($L$) in the operator $\hat{\rho}^{L}_{\Delta J,t_z}$, stands for longitudinal component, $Y_{\Delta J,M_{\Delta J}}(\Omega_{r_k})$ and $\delta(r-r_k)$ are the spherical harmonic and Dirac delta functions, respectively. The reduced matrix element of the longitudinal transition density operator in Eq. (1) can be expressed as [25]:

$$\left\langle J_f \left\| \hat{\rho}^{L}_{\Delta J,t_z}(\vec{r}) \right\| J_i \right\rangle = \frac{1}{\sqrt{4\pi(2J_i+1)}} \times \sum_{ab} OBDM(J_f, J_i, \Delta J, a, b, t_z) \left\langle j_a \left\| Y_{\Delta J} \right\| j_b \right\rangle \times R_{n_a l_a}(r) R_{n_b l_b}(r) \quad (2)$$

where $a$ and $b$ label single-particle states

for the considered shell model space and are specified by:

$|p\rangle = |n_p l_p\rangle |j_p m_p\rangle$, (the state $p$ represents either $a$ or $b$)

The states $|J_i\rangle$ and $|J_f\rangle$ are characterized by the model space wave functions. In Eq. (2), $R_{n_p l_p}(r)$ is the radial part of the harmonic oscillator wave function, $\langle j_a \| Y_{\Delta J} \| j_b \rangle$ is the reduced matrix element of the spherical harmonics and $OBDM(J_f, J_i, \Delta J, a, b, t_z)$ is the proton $(t_z = 1/2)$ or neutron $(t_z = -1/2)$ one-body density matrix element given by the second quantization notation as [25]:

$$OBDM(J_f, J_i, \Delta J, a, b, t_z) = \frac{\langle J_f \| [a^+_{a,t_z} \otimes \tilde{a}_{b,t_z}]^{\Delta J} \| J_i \rangle}{\sqrt{2\Delta J + 1}} \quad (3)$$

As the *spsdpf*- and *HASP* ($2s_{1/2}$, $1d_{3/2}$, $2p_{3/2}$, and $1f_{7/2}$ orbits)-shell wave functions (generated in the present study with WBP [26] and HASP [27] interactions, respectively), have good isospin, it is appropriate to evaluate the *OBDM* elements by means of isospin-reduced matrix elements. The relation between these tripled-reduced *OBDM* and the proton or neutron *OBDM* of Eq. (2) is given by [28]:

$$OBDM(t_z) = (-1)^{T_f - T_z} \sqrt{2} \begin{pmatrix} T_f & 0 & T_i \\ -T_z & 0 & T_z \end{pmatrix} \times$$
$$OBDM(\Delta T = 0)/2 + 2t_z (-1)^{T_f - T_z} \sqrt{6} \begin{pmatrix} T_f & 1 & T_i \\ -T_z & 0 & T_z \end{pmatrix} \times$$
$$OBDM(\Delta T = 1)/2 \quad (4)$$

The tripled-reduced $OBDM(\Delta T)$ elements are given in terms of the second quantization notation as [28]:

$$OBDM(i, f, \Delta J, \alpha, \beta, \Delta T) = \frac{\langle \Gamma_f \| [a^+_\alpha \otimes \tilde{a}_\beta]^{\Delta J, \Delta T} \| \Gamma_i \rangle}{\sqrt{2\Delta J + 1}\sqrt{2\Delta T + 1}} \quad (5)$$

Here, Greek symbols are utilized to indicate quantum numbers in coordinate space and isospace (i.e., $\Gamma_i \equiv J_i T_i$ and $\Gamma_f \equiv J_f T_f$).

The $OBDM(\Delta T)$ elements contain all the information about transitions of a given multipolarities which are embedded in the model wave functions. To obtain these *OBDM* elements, shell model calculations are performed using realistic effective interactions of WBP (for core nucleons of $^{22}$C) and HASP (for outer two-neutron halo in $^{22}$C).

For the ground state density distribution, we have $J_i = J_f$, $\Delta J = 0$, then Eq. (2) reduces to the following [25]:

$$\rho_{t_z}(r) = \frac{1}{\sqrt{4\pi(2J_i + 1)}} \times \sum_{ab} OBDM(J_i, J_i, 0, a, b, t_z) \times \langle j_a \| Y_0 \| j_b \rangle R_{n_a l_a}(r) R_{n_b l_b}(r). \quad (6)$$

where $\rho_{t_z}(r) = \langle J_i \| \hat{\rho}^L_{\Delta J = 0, t_z}(\vec{r}) \| J_i \rangle$.

As halo nuclei are oversized and easily broken systems consisting of a compact core plus a number of outer nucleons loosely bound and spatially extended far from the core, it is suitable to separate the ground state density distribution of Eq. (6) into two parts. The first part is connected to the core nucleons while the second part is connected to the halo (outer) nucleons, i.e.:

$$\rho_m(r) = \rho^{core}(r) + \rho^{halo}(r). \quad (7)$$

where the subscript (m) in Eq. (7) denotes matter. Moreover, Eq. (7) may also be expressed as:

$$\rho_m(r) = \rho_p(r) + \rho_n(r), \quad (8)$$

where $\rho_p(r)$ and $\rho_n(r)$ are the ground state proton and neutron densities of halo nuclei and expressed as:

$$\rho_p(r) = \rho_p^{core}(r) + \rho_p^{halo}(r) \quad (9)$$

and

$$\rho_n(r) = \rho_n^{core}(r) + \rho_n^{halo}(r). \quad (10)$$

The normalization condition of the above ground state densities is given by:

$$g = 4\pi \int_0^\infty \rho^g(r) r^2 dr. \quad (11)$$

Here, $\rho^g(r)$ represents one of the following densities: $\rho_m(r)$, $\rho^{core}(r)$, $\rho^{halo}(r)$, $\rho_p(r)$, $\rho_n(r)$. In that case, the parameter $g$ represents, correspondingly, one of the following quantities: the nuclear mass (*A*), the number of core nucleons, the number of halo nucleons, the total number of protons and the total number of neutrons of halo nuclei. The rms radii of the corresponding above densities are given by [29]:

$$< r^2 >_g^{1/2} = \frac{4\pi}{g} \int_0^\infty \rho^g(r) r^4 dr. \quad (12)$$

The PWBA is used to study the elastic electron scattering form factors from considered nuclei. In the PWBA, the incident and scattered electron waves are represented by plane waves. The elastic proton form factor is simply given by the Fourier-Bessel transformation of the ground state proton density distribution, i.e. [29]:

$$F(q) = \frac{4\pi}{Z} \int_0^\infty \rho_p(r) j_0(qr) r^2 dr \quad (13)$$

where $j_0(qr)$ is the spherical Bessel function of order zero and $q$ is the momentum transfer from the incident electron to the target nucleus.

In the limit $q \to 0$, the target nucleus will be characterized as a point particle. Accordingly, using Eq. (13) with the help of Eq. (9), the proton form factor of this target nucleus will be equal to unity (i.e. $F(q \to 0) = 1$).

**Results and Discussion**

The TFSM approach [23, 24] is employed to study the ground state proton, neutron and matter density distributions, the proton, neutron and matter rms radii and elastic nucleon form factors of the unstable $^{22}$C nucleus. The single particle harmonic oscillator wave functions are used with two different oscillator size parameters $b_{core}$ and $b_{halo}$. To obtain the OBDM elements of the core and halo parts, we perform shell model calculations via the computer code OXBASH [30].

$^{22}$C nucleus is a two-neutron Borromean halo nucleus composed of the core $^{20}$C nucleus plus two loosely bound neutrons surrounding the core; these outer two neutrons are considered to move in the *sd*-shell model space. The separation energy of the outer (halo) two neutrons is measured experimentally and found to be $S_{2n} = 420 \pm 940 KeV$ [17, 18]. The oscillator size parameters for core and outer (halo) two neutrons are chosen to be $b_{core}$=2.7 fm and $b_{halo}$=5.4 fm to reproduce the experimental neutron rms radius ($5.4 \pm 0.9\ fm$) [17] of $^{22}$C nucleus. Using these values of $b_{core}$ and $b_{halo}$, the calculated neutron, proton and matter rms radii are 5.609, 3.974 and 4.783 fm, respectively. It is so clear that the

calculated neutron rms radius is in very good agreement with the experimental value. The difference between the calculated overall neutron and proton rms radii is 1.635 fm. This difference indicates a halo structure in $^{22}$C nucleus.

In present study, we assume that the core neutrons and protons (i.e., $^{20}$C core of $^{22}$C) move within the *spsdpf* −model space. To obtain the OBDM elements of the core part, shell model calculations are performed in the above mentioned space with $(0+2)\hbar\omega$ truncations using the realistic interaction of WBP [26]. For the outer (halo) two neutrons in $^{22}$C, we perform shell model calculations for two neutrons moving in the HASP model space of $1d_{3/2}$, $2s_{1/2}$, $2p_{3/2}$, and $1f_{7/2}$ orbitals using the realistic effective interaction of the HASP [27].

The neutron ($\rho_n(r)$) and proton ($\rho_p(r)$) densities (in fm$^{-3}$) of $^{22}$C are plotted in Fig. 1 as a function of $r$ (in fm). The solid, dashed, and dash-dotted curves are the calculated neutron density distributions when the outer two neutrons of $^{22}$C move in HASP model space, in the pure $2s_{1/2}$ and $1d_{3/2}$ -orbits, respectively. The plus symbols are the calculated proton density distribution. The filled circles curve is the experimental neutron density distribution [17] extracted from the fitting of Glauber model with experimental cross sections using HO+Yukawa type density function. Fig. 1 shows that the tendency of the solid and dash-dotted distributions is approximately the same during the entire range of considered *r*. The long tail behavior is apparently seen in these distributions of neutron densities. This behavior is associated to the existence of the outer two neutrons of $^{22}$C in the halo $2s_{1/2}$-orbit.

The calculated proton density distribution of $^{22}$C shown in Fig. 1 demonstrates a steep slope behavior because there are no protons found in the halo orbits (all protons of $^{22}$C are found within their core only). It is useful to remark that the halo phenomenon in $^{22}$C is connected to the matter and neutron densities and not to the proton density.

Fig. 2 shows the same calculations as in Fig.1, but here for the matter distribution $\rho_m(r)$. The solid curve is the calculated matter density obtained with the assumption that the outer two neutrons of $^{22}$C move in the HASP model space. The dash-dotted curve is the calculated matter density when the outer two neutrons move in the pure $2s_{1/2}$-orbit. It is clear that both the solid and the dash-dotted distributions, in which their behavior is nearly the same throughout the whole range of *r*, show the long tail behavior (which is a distinctive feature of halo nuclei).

The ground state occupation numbers of the outer two neutrons of $^{22}$C, obtained by the HASP model space calculations using the HASP interaction, are 0.284 for $(1d_{3/2})^2$, 1.2 for $(2s_{1/2})^2$, 0.39 for $(1f_{7/2})^2$ and about 0.126 is for $(2p_{3/2})^2$. Inspection of these occupation numbers and also of calculated matter densities shown in Fig. 2 leads to the conclusion that the structure of the $^{22}$C nucleus has a $2s_{1/2}$-dominant configuration.

In Fig. 3, the matter densities of unstable $^{22}$C and stable $^{14}$C are displayed by the solid and dash-dotted curves, respectively. The matter density distribution of unstable $^{22}$C is that calculated in Fig. 2. The distribution of stable $^{14}$C shown in Fig. 3 is calculated by means of the WBP interaction, where all nucleons of $^{14}$C are assumed to move within the *spsdpf* −model space with $(0+2)\hbar\omega$ truncations.

It is so clear from Fig. 3 that the matter densities of $^{22}$C and $^{14}$C nuclei are diverse. As the outer (halo) two neutrons in $^{22}$C are weakly bound, the neutron density distribution of the last two neutrons has a longer tail than that of $^{14}$C nucleus. This can

be seen obviously from the comparison between the matter density distributions of both nuclei shown in Fig. 3.

To seek out if the long tail behavior of the matter density distribution of the neutron-rich nuclei demonstrates noticeable effects in the process of elastic electron scattering, elastic nucleon form factors for unstable neutron-rich $^{22}$C and stable $^{14}$C are calculated by means of the PWBA.

In Fig. 4, the dependence of the squared nucleon form factor $|F(q)|^2$ on the momentum transfer $q$ (in fm$^{-1}$) is exhibited, where the input matter density distributions are those of Fig. 3. The calculated nucleon form factors of the stable $^{14}$C and unstable $^{22}$C nuclei are displayed by the dash-dotted and solid curves, respectively. The experimental elastic charge form factors of stable $^{14}$C [31] are displayed by open circles for comparison. Fig. 4 demonstrates that the behavior of the calculated nucleon form factors (the dash-dotted curve) for $^{14}$C is consistent with the data. In addition, the magnitudes of the calculated form factors of $^{14}$C underestimate slightly the data at the region of momentum transfer $1.4 \le q \le 1.75$ fm$^{-1}$ around the first observable diffraction minimum, while at other regions of momentum transfer they almost coincide with the data. In general, the calculated form factors of $^{14}$C are in reasonable agreement with all experimental data presented in the range of $q \le 2.2$ fm$^{-1}$. However, this comparison gives the conclusion that the PWBA can reproduce the experimental data of elastic electron scattering on the stable $^{14}$C. The elastic electron scattering nucleon form factors of unstable neutron-rich nuclei $^{22}$C can be also discussed. It is so clear from Fig. 4 that there are significant differences between the calculated form factors of $^{22}$C (the solid curve) and $^{14}$C (the dash-dotted curve). The solid curve of unstable $^{22}$C has two diffraction minima (located at momentum transfer $q = 1.08$ and $q = 1.6$ fm$^{-1}$) and two diffraction maxima (located at $q = 1.2$ and $q = 1.78$ fm$^{-1}$). The locations of the first and second minima of $^{22}$C have an inward shifts of approximately 0.62 and 0.14, respectively as compared with the observable diffraction minimum of $^{14}$C.

As mentioned before, the elastic nucleon form factor in the nucleus is simply connected to its nucleon density distribution. For that reason, the difference between the nucleon form factors of $^{22}$C and that of $^{14}$C is owing to the different matter density distributions of the two nuclei. The difference between the matter density distributions of $^{22}$C and $^{14}$C is essentially caused by two reasons; the first is due to the effect of the neutron skin of the core $^{20}$C and the second is due to the difference in the neutron density distribution of the last two neutrons in both $^{14}$C and $^{22}$C nuclei.

To analyze the effect of the long tail of the matter density distribution on elastic electron-nucleus scattering, one requires identifying which part of the form factor is responsive to the tail of the matter density distribution. It is recognized from the fitting to the experimental data of $^{12}C$ [32] and $^{32}S$ [33] that the form factors in the region of momentum transfer $1 \le q \le 3$ fm$^{-1}$ are responsive to the change of the tail part of the density distribution, whereas those at the region of high momentum transfer $q \ge 3$ fm$^{-1}$ are responsive to the change of the central part of the density distribution. It is expected that the conclusions of $^{12}C$ [32] and $^{32}S$ [33] work as well for C isotopes. Therefore, one may attribute the difference of the calculated form factors at $1 \le q \le 3$ fm$^{-1}$ between $^{22}$C and $^{14}$C (Fig. 4) to the influence of the long tail of the neutron density distribution of $^{22}$C while that at $q \ge 3$ fm$^{-1}$ to the influence of the neutron density difference at the central parts.

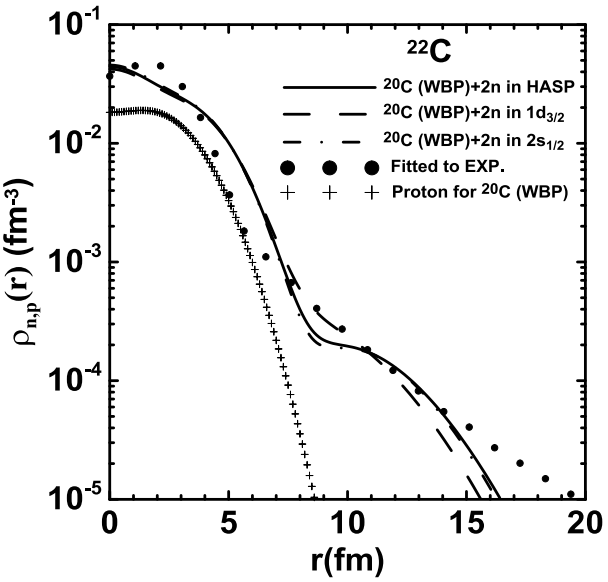


***Fig. 1: The dependence of proton and neutron density distributions (in $fm^{-3}$) on r (in fm) of $^{22}C$ nucleus. The filled circles are the fitted to experiment [17].***

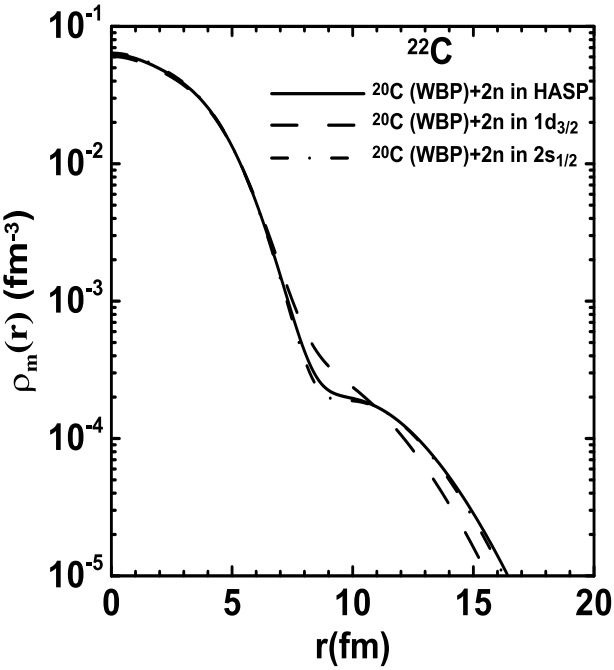


***Fig. 2: The same as in figure 1, but for the matter density distribution.***

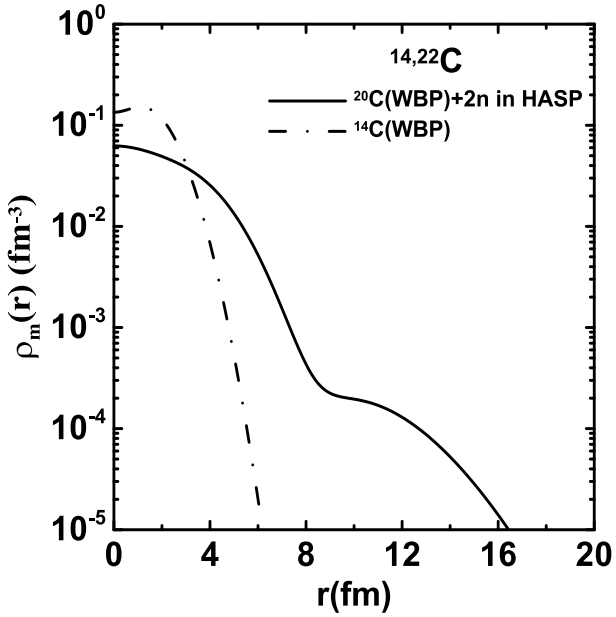


***Fig. 3: The calculated matter densities for halo $^{22}C$ compared with that of stable $^{14}C$***

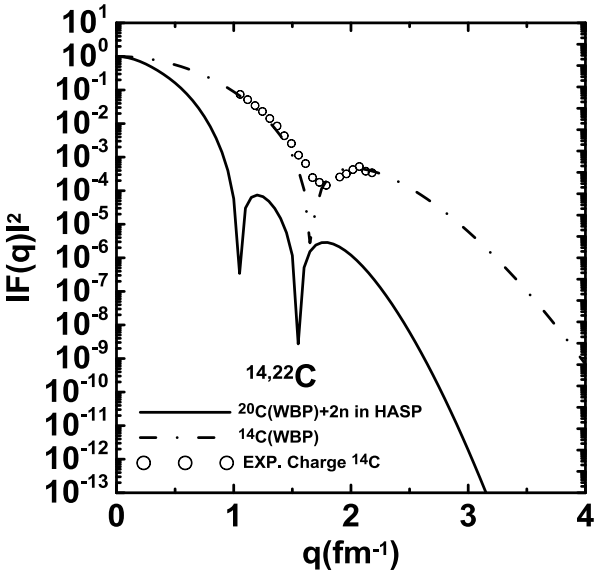


***Fig. 4: The calculated nucleon form factors for halo $^{19}C$ compared with that calculated for stable $^{13}C$. The open circles represent the experimental charge form factor for $^{13}C$ [31].***

## Conclusions

The long tail behavior, considered as a distinctive feature of halo nuclei, is evidently revealed in the calculated neutron and matter density distributions. Besides, the noticeable difference that is found between the calculated overall proton and neutron

rms radii of $^{22}$C nuclei also indicates a halo structure. It is found that the structure of $^{22}$C nucleus has $(2s_{1/2})^2$- dominant configuration. The difference observed between the nucleon form factors of $^{22}$C and $^{14}$C is generally caused by the difference in the matter density distribution resulting from the existing of the neutron skin in the core of $^{20}$C and from the difference in the neutron densities of the last two neutrons in both $^{14}$C and $^{22}$C nuclei. Because the difference of the nucleon form factors between the stable nucleus and its neutron drip-line isotope has observable effects, we regard that elastic electron scattering is an efficient tool to examine neutron-halo phenomena in neutron-rich nuclei.

**Acknowledgment**

The authors would like to express their thanks to Professor B. A. Brown of the National Superconducting Cyclotron Laboratory, Michigan State University, for providing the computer code OXBASH.

**References**

[1] I. Tanihata, H. Hamagaki, O. Hashimoto, Y.Shida, N. Yoshikawa, K. Sugimoto, O.Yamakawa, T. Kobayashi, and N. Takahashi,Phys. Rev. Lett., 55 (1985) 2676.

[2] I. Tanihata, H. Hamagaki, O. Hashimoto, S. Nagamiya, Y. Shida, N. Yoshikawa, O.Yamakawa, K. Sugimoto, T. Kobayashi, D. E. Greiner, N. Takahashi, and Y. Nojiri, Phys. Lett., B 160 (1985) 380.

[3] P. G. Hansen and B. Jonson, Europhys. Lett.,4 (1987) 409.

[4]I. Tanihata, T. Kobayashi, O. Yamakawa, S.Shimoura, K. Ekuni, K. Sugimoto, N.Takahashi, T. Shimoda, and H. Sato, Phys.Lett., B 206 (1988) 592.

[5] M. V. Zukov B. V. Danilin, D. V. Fedorov, J.M. Bang, I. J. Thompson, and J. S. Vaagen.,Phys. Rep. 231(1993)151.

[6] J. S. Al-Khalili, J. A. Tostevin, and I. J. Thompson, Phys. Rev. C 54 (1996) 1843.

[7] Technical Proposal for the Design, Construction, Commissioning, and Operation of the ELISe setup, Haik Simon, GSI Internal Report, Dec. 2005.

[8] T. Suda, K. Maruyama, Proposal for the RIKEN beam factory, RIKEN,2001; M. Wakasugi, T. Suda, Y. Yano, Nucl.Inst. Meth. Phys., A532 (2004) 216.

[9] M. M. Sharma, S. Mythili, and A. R. Farhan, Phys. Rev., C 59 (1999) 1379.

[10] A. Ozawa, O. Bochkarev, L. Chulkov, D.Cortina, H. Geissel, M. Hellstrom, M.Ivanov, R. Janik, K. Kimura, T. Kobayashi, A. A. Korsheninnikov, G. Munzenberg, F.Nickel, Y. Ogawa, A. A. Tanihata, M.Winkler, and K. Yoshida, Nucl.Phys., A 691 (2001) 599.

[11] Yoshiko Kanada-EN'YO and Hisashi Horiuchi, arXiv: nucl-th 0107044v1 16 Jul 2001.

[12] H. Sagawa, X. R. Zhou, X. Z. Zhang and T.Suzuki, Phys. Rev., C 70 (2004) 054316-1.

[13] Dao T. Khoa, Hoang Sy Than, Tran Hoai Nam, Marcella Grasso and Nguyen Van Giai, Phys. Rev.,C 69 (2004) 044605-1.

[14] G. Gangopadhyay and Subinit Roy, J. Phys., G 31 (2005) 1111.

[15] W. Horiuchi and Y. Suzuki, Phys. Rev., C 74 (2006) 034311-1.

[16] B. Abu-Ibrahim, W. Horiuchi, A. Kohama, and Y. Suzuki, Phys. Rev., C 77 (2008) 034607-1.

[17] K. Tanaka, T. Yamaguchi, T. Suzuki, T. Ohtsubo, M. Fukuda, D. Nishimura, M. Takechi, K. Ogata, A. Ozawa, T.Izumikawa, T. Aiba, N. Aoi, H. Baba, Y.Hashizume, K. Inafuku, N. Iwasa, K.Kobayashi, M. Komuro, Y. Kondo, T. Kubo, M. Kurokawa, T. Matsuyama, S. Michimasa, T.Motobayashi, T.Nakabayashi, S. Nakajima, T. Nakamura, H. Sakurai, R. Shinoda, M. Shinohara, H.Suzuki, E. Takeshita, S. Takeuchi, Y. Togano, K. Yamada, T. Yasuno, and M. Yoshitake, Phys. Rev. Lett., 104 (2010) 062701-1.

[18] Manjari Sharma, A. Bhagwat, Z. A. Khan,W. Haider, and Y. K. Gambhir, Phys. Rev., C 83 (2011) 031601(R).
[19] P. Navratil and B. R. Barrett, Phys. Rev., C54 (1996) 2986.
[20] P. Navratil and B. R. Barrett, Phys. Rev., C57 (1998) 3119.
[21] E. Caurier and P. Navratil, Phys. Rev., C73 (2006) 021302-1(R).
[22] S. Karataglidis, K. Amos, P. Fraser, L. Canton, J. P. Svenne, Nucl. Phys., A813 (2008) 235.
[23] T. T. S. Kuo, H. Muether, and K. Amir-Azimi-Nili, Nucl. Phys., A606 (1996) 15.
[24] T. T. S. Kuo, F. Krmpotic, and Y. Tzeng, Phys. Rev. Lett., 78 (1997) 2708.
[25] B. A. Brown, R. Radhi, and B. H. Wildenthal, Phys. Rep., 101 (1983) 313.
[26] E. K. Warburton, and B. A. Brown, Phys.Rev., C 46 (1992) 923.
[27] H.Hasper, Phys. Rev.,C19 (1979) 1482.
[28] R. A. Radhi, Ph.D.Thesis, Michigan state University, USA, (1983).
[29] L. R. B. Elton, "Nuclear Sizes", Oxford University Press (1961).
[30] Brown B. A., Etchegoyen A., Godwin N. S.,Rae W. D. M., Richter W. A., Ormand W.E., Warburton E. K., Winfield J. S., Zhao L., Zimmerman C. H. 2005. Oxbash for Windows PC. MSU-NSCL report number1289.
[31] F. J. Kline, Hall Crannell and James T. O'Brien, Nucl. Phys., A209 (1973) 381.
[32] I. Sick and J. S. McCarthy, Nucl. Phys., A150 (1970) 631.
[33] G. C. Li, M. R. Yearian, and I. Sick, Phys. Rev., C 9 (1974) 1861.